



Communication

Development of a Radiofluorinated Adenosine A_{2B} Receptor Antagonist as Potential Ligand for PET Imaging

Marcel Lindemann ^{1,†} , Rareş-Petru Moldovan ^{1,†} , Sonja Hinz ², Winnie Deuther-Conrad ¹ , Daniel Gündel ¹ , Sladjana Dukic-Stefanovic ^{1,3}, Magali Toussaint ¹, Rodrigo Teodoro ¹ , Cathleen Juhl ³, Jörg Steinbach ¹, Peter Brust ¹ , Christa E. Müller ² and Barbara Wenzel ^{1,*}

¹ Department of Neuroradiopharmaceuticals, Institute of Radiopharmaceutical Cancer Research, Helmholtz-Zentrum Dresden-Rossendorf, 04318 Leipzig, Germany; marcel.lindemann@uit.no (M.L.); r.moldovan@hzdr.de (R.-P.M.); w.deuther-conrad@hzdr.de (W.D.-C.); d.guendel@hzdr.de (D.G.); s.dukic-stefanovic@hzdr.de (S.D.-S.); m.toussaint@hzdr.de (M.T.); r.teodoro@hzdr.de (R.T.); j.steinbach@hzdr.de (J.S.); p.brust@hzdr.de (P.B.)

² Pharma Center Bonn, Pharmaceutical & Medicinal Chemistry, Pharmaceutical Institute, University of Bonn, 53121 Bonn, Germany; Sonja.Hinz@uni-wh.de (S.H.); christa.mueller@uni-bonn.de (C.E.M.)

³ ROTOP Pharmaka GmbH, 01328 Dresden, Germany; service@rotop-pharmaka.de

* Correspondence: b.wenzel@hzdr.de; Tel.: +49-341-2341794637

† These authors have contributed to this work equally.

Received: 6 April 2020; Accepted: 28 April 2020; Published: 30 April 2020



Abstract: The adenosine A_{2B} receptor has been proposed as a novel therapeutic target in cancer, as its expression is drastically elevated in several tumors and cancer cells. Noninvasive molecular imaging via positron emission tomography (PET) would allow the in vivo quantification of this receptor in pathological processes and most likely enable the identification and clinical monitoring of respective cancer therapies. On the basis of a bicyclic pyridopyrimidine-2,4-dione core structure, the new adenosine A_{2B} receptor ligand **9** was synthesized, containing a 2-fluoropyridine moiety suitable for labeling with the short-lived PET radionuclide fluorine-18. Compound **9** showed a high binding affinity for the human A_{2B} receptor ($K_i(A_{2B}) = 2.51$ nM), along with high selectivities versus the A₁, A_{2A}, and A₃ receptor subtypes. Therefore, it was radiofluorinated via nucleophilic aromatic substitution of the corresponding nitro precursor using [¹⁸F]F⁻/K_{2.2.2}/K₂CO₃ in DMSO at 120 °C. Metabolic studies of [¹⁸F]**9** in mice revealed about 60% of radiotracer intact in plasma at 30 minutes p.i. A preliminary PET study in healthy mice showed an overall biodistribution of [¹⁸F]**9**, corresponding to the known ubiquitous but low expression of the A_{2B} receptor. Consequently, [¹⁸F]**9** represents a novel PET radiotracer with high affinity and selectivity toward the adenosine A_{2B} receptor and a suitable in vivo profile. Subsequent studies are envisaged to investigate the applicability of [¹⁸F]**9** to detect alterations in the receptor density in certain cancer-related disease models.

Keywords: A_{2B} adenosine receptor; adenosine; PET; fluorine-18; metabolism; radiofluorination

1. Introduction

Adenosine receptors belong to the family of G-protein-coupled receptors and are activated by the purine nucleoside adenosine, a precursor and degradation product of adenine nucleotides such as adenosine 5'-triphosphate (ATP). The effects of adenosine are mediated via the four receptor subtypes A₁, A_{2A}, A_{2B}, and A₃. Each of these exhibits distinct pharmacological properties, cell and tissue distribution, and intracellular signaling [1–3]. The adenosine A_{2B} receptor can be seen as unique as its activation requires high levels of adenosine with concentrations in the micromolar range [3–5],

accompanied by an ubiquitous expression at mostly moderate to low levels [3,6]. Therefore, in comparison with the other adenosine receptors, the function and physiological role of this low-affinity receptor has been sparsely characterized to date and is barely understood. However, in recent years, the involvement of the A_{2B} receptor in pathophysiological processes was discovered to be driven by the fact that extracellular concentrations of adenosine increase under certain pathological conditions such as hypoxia or inflammation [6–8]. In particular, the relevance of A_{2B} receptor in promoting cancer progression has been revealed via mechanisms such as tumor growth, angiogenesis, metastasis, and immunomodulation, and it has been shown that its expression can be drastically increased in tumors and cancer cells, as recently reviewed [6,9–11]. Moreover, current pharmaceutical studies indicate that the A_{2B} receptor might be particularly appropriate for cancer therapies in comparison to other adenosine receptor subtypes that show to some extent both pro- and antitumor effects [7,9,12]. Thus, the adenosine A_{2B} receptor is a highly relevant therapeutic target, although extensive and interdisciplinary research is still needed to gain a deeper understanding.

Noninvasive molecular in vivo imaging using positron emission tomography (PET) could be one tool used to approach this goal. For example, it would allow quantification of the A_{2B} receptor in pathological processes and probably enable clinical monitoring of A_{2B} -receptor-related cancer therapies. Therefore, the development of a suitable radioligand to target the adenosine A_{2B} receptor with high affinity and selectivity, accompanied by a suitable pharmacokinetic and metabolic profile in vivo is desired. In 2016, Petroni et al. [13] developed the first PET radiotracer for this receptor subtype, which was labeled with the short-lived radionuclide carbon-11 ($t_{1/2} = 20.4$ min). The authors investigated the compound in rats and concluded that it might represent a good candidate, but further characterization would be needed. We recently reported on the first PET radiotracer ($[^{18}\text{F}]\mathbf{1}$, Figure 1) labeled with the radionuclide fluorine-18 ($t_{1/2} = 109.8$ min) [14]. The radiotracer was designed using structural modification on the basis of a monocyclic pyrazine compound class published by Eastwood, Vidal, et al. [15], and resulted in a small series of fluorinated derivatives. The most appropriate candidate, **1**, showed a high binding affinity for the A_{2B} receptor ($K_i = 4.24$ nM). Despite its moderate selectivity (see data in Table 1), we synthesized the corresponding radiotracer $[^{18}\text{F}]\mathbf{1}$ for investigation of the pharmacokinetic profile of this monocyclic compound class in vivo. Rapid metabolic degradation of $[^{18}\text{F}]\mathbf{1}$ was observed in mice, with the formation of a radiometabolite generated by the cleavage of the amide bond which, besides the moderate selectivity, might cause difficulties for specific imaging.

Therefore, the aim of the present study was to develop a new radiofluorinated PET tracer possessing (i) a higher selectivity for the adenosine A_{2B} receptor versus the other subtypes, and (ii) a suitable metabolic profile in vivo. For this purpose, we selected the bicyclic pyridopyrimidine-2,4-dione core as the lead structure (**2** in Figure 1), which was previously described to fulfill both criteria [16]. The authors reported for **2** a K_i value of 1 nM at the A_{2B} receptor (see Table 1) and a high metabolic stability, determined via in vitro studies with rat hepatic microsomes [16]. In order to introduce the required radiofluoro atom, the pyrimidine ring of **2** was substituted by a 2-fluoropyridine ring representing a very common heteroaromatic motive for ^{18}F -radiolabeling reactions ($[^{18}\text{F}]\mathbf{9}$, Figure 1). For a straightforward radiosynthesis using nucleophilic aromatic substitution with $[^{18}\text{F}]\text{fluoride}$, a precursor compound was developed containing a nitro group as a suitable leaving group (**10**, Scheme 1).

This communication describes (i) the organic and radiosynthesis of the new A_{2B} receptor PET ligand $[^{18}\text{F}]\mathbf{9}$, (ii) the in vitro binding data of the non-radioactive ligand **9** toward all four adenosine receptor subtypes, and (iii) preliminary results for $[^{18}\text{F}]\mathbf{9}$ regarding in vivo metabolism and biodistribution.

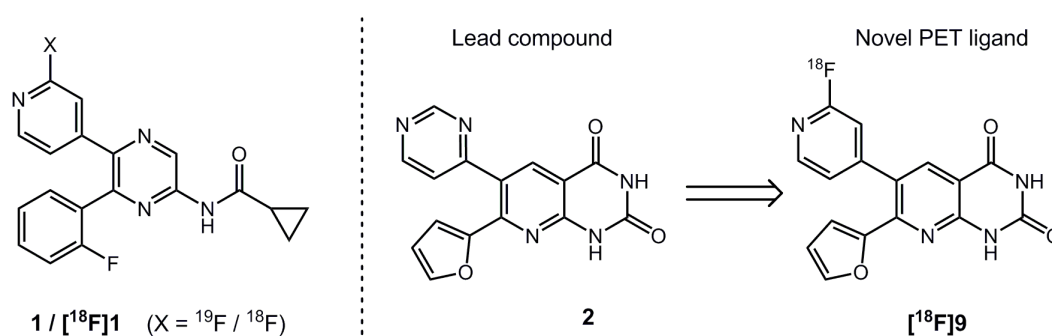


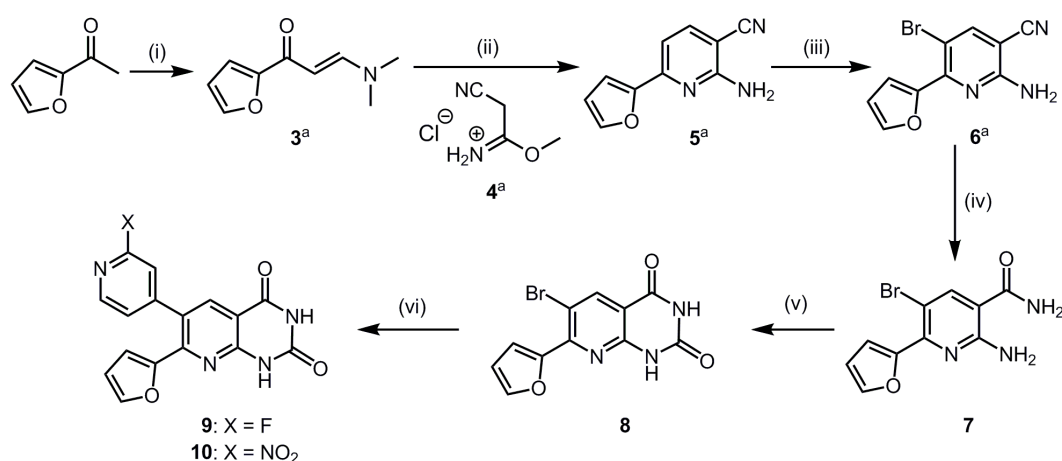
Figure 1. Molecular structures of the previously radiofluorinated PET ligand [^{18}F]**1** [14], the selected new bicyclic lead compound **2** [16], and the newly developed $\text{A}_{2\text{B}}$ receptor PET ligand [^{18}F]**9**.

2. Results and Discussion

2.1. Organic Synthesis and In Vitro Binding Studies

In order to investigate the influence of the substitution of the pyrimidine ring in lead compound **2** by the 2-fluoropyridine ring in target compound **9** on the affinity and selectivity toward the $\text{A}_{2\text{B}}$ receptor, **2** was synthesized as a reference compound. This synthesis was performed according to the procedures described by Eastwood et al. [16,17]. For the synthesis of the new $\text{A}_{2\text{B}}$ receptor ligand **9**, another strategy was chosen, which is shown in Scheme 1. Briefly, the three-fold substituted pyridine core **5** was built up via a two-step synthesis sequence starting from 2-acetyl furane, which was treated with *N,N*-dimethylformamide dimethyl acetal to obtain compound **3** [18]. Further reaction of **3** with the hydrochloride salt **4** and ammonium acetate gave **5**, which was selectively brominated to obtain compound **6**. Derivatives **3–6** have been previously described and the reported synthesis procedures [18–20] were adopted with slight modifications (see Supplementary material). In the next step, the cyano group was hydrolyzed using hydrogen peroxide under basic conditions to obtain the amide **7**, which was then cyclized to **8** by deprotonation with sodium hydride and subsequent reaction with *N,N*-carbonyldiimidazole. The obtained pyridopyrimidine-2,4-dione **8** was used for a Suzuki coupling reaction [21,22] with 2-fluoro pyridine-4-boronic acid to achieve the desired compound **9**. The bicyclic intermediate **8** was also used for the synthesis of the precursor compound **10**. The required 2-nitropyridine-4-boronic acid pinacol ester was synthesized via a Miyaura borylation [23] of the corresponding bromo-substituted nitropyridine and subsequently coupled in situ with **8** in a Suzuki reaction, affording the nitro precursor **10**.

The binding affinities of **2** and **9** at the four human adenosine receptor subtypes $\text{A}_{2\text{B}}$, $\text{A}_{2\text{A}}$, A_1 , and A_3 , presented in Table 1, were determined in competitive binding assays using appropriate radioligands and membrane preparations of Chinese hamster ovary (CHO) cells or human embryonic kidney (HEK) cells, respectively, recombinantly expressing the corresponding human receptor subtype.



Scheme 1. Synthesis of the new A_{2B} receptor ligand **9** and its precursor for radiofluorination **10**. Reaction conditions: (i) *N,N*-dimethylformamide dimethyl acetal, reflux, 5.5 h, 90%, (ii) **4**, NH_4OAc , MeOH, reflux, 12 h, 70%, (iii) *N*-bromosuccinimide (NBS), *N,N*-dimethylformamide (DMF), 12 hours, rt, 77%, (iv) 6 M NaOH, H_2O_2 , 50 °C, 5 h, 45%; (v) a) NaH, DMF, 30 min, rt, b) *N,N*-carbonyldiimidazole, 90 °C, 2 h, 50%; (vi) **9**: 2-fluoro pyridine-4-boronic acid, 2 M Cs_2CO_3 , $[\text{Pd}(\text{dppf})\text{Cl}_2]$, 1,4-dioxane, 90 °C, 2 h, 59%; **10**: (a) 4-bromo-2-nitropyridine, 4,4,4',4',5,5,5',5'-octamethyl-2,2'-bis(1,3,2-dioxaborolane), KOAc and $[\text{Pd}(\text{dppf})\text{Cl}_2]$, 90 °C, 1 h (b) 2 M Cs_2CO_3 , $[\text{Pd}(\text{dppf})\text{Cl}_2]$, 90 °C, 1 h, 9%. ^a The synthesis of compounds **3–6** has been previously reported [18–20] and was performed accordingly with slight modifications, as described in the Supplementary material.

The in-house-determined binding data of compound **2** corresponded to the values reported by Eastwood et al. [16] and thus confirmed its high affinity and selectivity for the A_{2B} receptor. The substitution of the pyrimidine ring in **2** by a 2-fluoropyridine ring in the new derivative **9** did not affect the binding affinity for the A_{2B} receptor, as indicated by the K_i value of 2.51 nM obtained for both compounds. Accordingly, compound **9** possesses a two-fold higher binding affinity for the A_{2B} receptor in comparison to our recently developed ligand **1**. Moreover, the selectivity of **9** regarding the two adenosine receptor subtypes A_1 and A_{2A} was considerably higher than that of **1** (K_i ratios of 43 and 59 versus 13 and 4.5, resp.; see Table 1). Due to a slight increase in the binding affinity of **9** for the A_3 receptor, the selectivity regarding this off-target was slightly decreased but still in a suitable range for the purpose of specific imaging (K_i ratio of 114).

Table 1. K_i values of **1**, lead compound **2**, and the new fluorinated derivative **9** at the four human adenosine receptor subtypes along with the corresponding selectivity ratios.

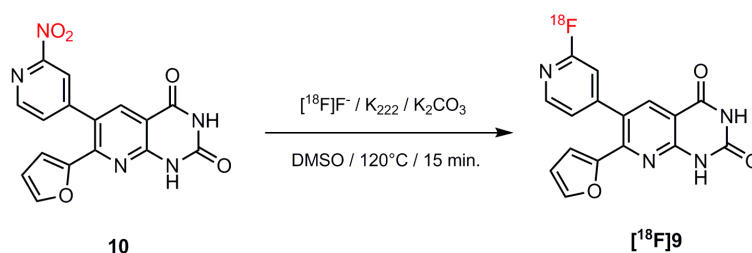
Compound	K_i in nM ^a				Selectivity Ratio $K_i(A_x)/K_i(A_{2B})$		
	A_{2B}	A_{2A}	A_1	A_3	A_{2A}/A_{2B}	A_1/A_{2B}	A_3/A_{2B}
1	4.24 ± 0.04 ^b	55.0 ± 6.1 ^b	19.0 ± 5.2 ^b	796 ± 26 ^b	13	4.5	188
2	2.51 ± 1.1 1 ± 0 ^c	98.8 ± 28.3 181 ± 25 ^c	> 1000 1727 ± 617 ^c	> 1000 6267 ± 2322 ^c	39	> 400	> 400
9	2.51 ± 0.58	107 ± 15	149 ± 26	286 ± 10	43	59	114

^a Data are means \pm SEM of three independent assays, each performed in duplicate. Competitive binding assays with $[\text{}^3\text{H}]\text{PSB-603}$ (A_{2B}), $[\text{}^3\text{H}]\text{MSX-2}$ (A_{2A}), $[\text{}^3\text{H}]\text{CCPA}$ (A_1), and $[\text{}^3\text{H}]\text{PSB-11}$ (A_3) as radioligands and membranes obtained from CHO or HEK cells stably expressing the corresponding human adenosine receptor. ^{b,c} Data are taken from References [14,16], resp.

2.2. Automated Radiosynthesis and Characterization of $[\text{}^{18}\text{F}]\text{9}$

The radiolabeling of $[\text{}^{18}\text{F}]\text{9}$ was performed via a nucleophilic aromatic substitution reaction of the nitro group of precursor **10** and $[\text{}^{18}\text{F}]\text{fluoride}$ (Scheme 2), which was azeotropically dried using

the kryptofix/potassium carbonate system and acetonitrile (ACN). Based on our former experiments with compound [^{18}F]1 [14], we selected dimethyl sulfoxide (DMSO) as the most promising solvent. All radiolabeling experiments were performed with a very low amount of precursor (about 0.5 mg).



Scheme 2. ^{18}F -labeling of precursor **10** to obtain [^{18}F]**9**.

The complete radiosynthesis of [^{18}F]**9** was accomplished in a remotely controlled synthesis module (TRACERlab FX2 N from GE Healthcare). The synthesizer setup is described in detail in the Materials and Methods. Briefly, [^{18}F]fluoride was trapped on an anion exchange cartridge, eluted with aqueous potassium carbonate, and then azeotropically dried to obtain the [^{18}F]F $^-$ /K $_{2.2.2}$ /K $_2$ CO $_3$ complex. Radiofluorination of the precursor **10** was performed in DMSO for 15 min at 120 °C. In order to isolate [^{18}F]**9**, the crude reaction mixture was diluted with aqueous methanol and applied to a semi-preparative HPLC system (chromatogram in Figure S1 in Supplementary Material). The radiotracer fraction was collected at retention times in the range of 22–25 min and purified by solid-phase extraction using a C18 cartridge. Afterwards, [^{18}F]**9** was eluted from the cartridge and transferred out of the hot cell for concentration and formulation in sterile isotonic saline containing 10% ethanol. The entire process lasted about 80 min. With this procedure, [^{18}F]**9** could be reproducibly generated with a high radiochemical purity of $\geq 99\%$, reasonable radiochemical yields of $48\% \pm 4\%$ ($n = 4$) and molar activities of 10–32 GBq/ μmol ($n = 4$) at starting activities of 2–7 GBq. The identity of [^{18}F]**9** was confirmed by analytical radio-HPLC (Figure S2 in Supplementary Material) with co-injection of the corresponding non-radioactive reference compound **9**.

For estimation of the lipophilicity of [^{18}F]**9**, the shake-flask method with *n*-octanol and phosphate-buffered saline as a partition system was used, resulting in a logD value of 1.4 ± 0.1 ($n = 4$).

2.3. In Vivo Studies of [^{18}F]**9** in Mice

The metabolism of [^{18}F]**9** in vivo was investigated in CD-1 mice by taking blood and urine samples at 30 min post i.v. injection of the radiotracer ($n = 2$). Analysis of the respective samples was performed by micellar (MLC) and reversed-phase chromatography (RP-HPLC) as two complementary HPLC methods. MLC is also a reversed-phase HPLC mode, but it uses a mobile phase consisting of an aqueous solution with a surfactant above its critical micellar concentration. The formed micelles are able to dissolve the proteins and other components of a biological sample and therefore enable a direct injection of the plasma probe into the HPLC system without eliminating the tissue matrix [24]. In contrast, for RP-HPLC analysis, aliquots of the plasma samples were treated with a mixture of ACN/water to precipitate the proteins, resulting in recoveries of activity of about 93%.

In general, the results obtained with both methods were comparable. Figure 2 shows exemplary RP-HPLC and MLC chromatograms of a plasma and urine sample at 30 min p.i. Accordingly, intact radiotracer accounted for $\sim 60\%$ of the total activity in plasma, which was a considerably higher fraction of intact radiotracer in comparison to our former radiotracer [^{18}F]**1** (35% at 30 min p.i.) [14]. The main radiometabolite was slightly more polar than [^{18}F]**9** and was also found in the urine, indicating, along with a very high activity concentration (standardized uptake value (SUV) = 75), a renal excretion route for [^{18}F]**9**. Besides this main radiometabolite, a small fraction of more polar radioactive metabolites was observed in urine.

When comparing the chromatograms of the two HPLC methods, slight differences in the retention profile became evident, a phenomenon that is caused by the differences in the separation mechanisms of the two chromatographic systems. Moreover, the RP-HPLC chromatograms showed a lower fraction of a very polar radiometabolite (within the first 5 min retention time) compared to the MLC ones. Considering the plasma sample, this influenced the peak quantification and therefore resulted in a supposed slightly higher percentage of intact radiotracer using the RP-HPLC method. However, it is likely that this polar component could not be quantitatively extracted during the plasma work-up procedure used to generate the injection sample for RP-HPLC, as reflected by the non-quantitative recovery of 93%. Considering this small loss resulted in a calculated value of 60% of intact tracer for RP-HPLC, which was comparable to the MLC result. In a separate *in vitro* experiment, the quantitative recovery of the radiotracer could be shown using the same work-up procedure.

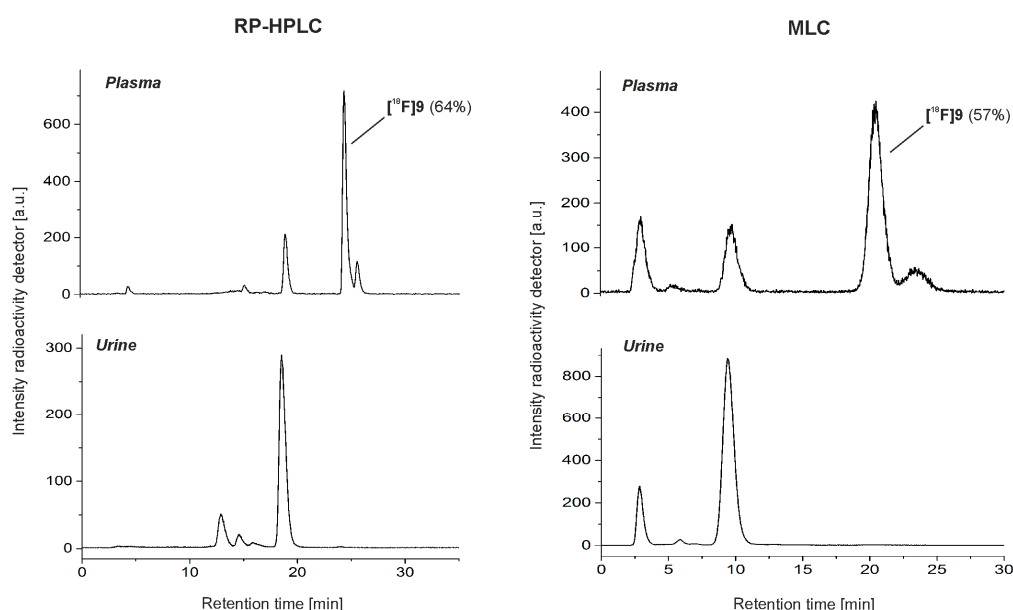


Figure 2. Exemplary RP-HPLC (left) and MLC (right) radio-chromatograms of mouse plasma and urine samples at 30 min p.i. of [^{18}F]9 (conditions RP-HPLC: Reprosil-Pur C18-AQ, 250 \times 4.6 mm, gradient with eluent mixture of ACN/20 mM aq. NH_4OAc , 1.0 mL/min; conditions MLC: Reprosil-Pur C18-AQ, 250 \times 4.6 mm, gradient with an eluent mixture of EtOH/100 mM aq. SDS/25 mM aq. $(\text{NH}_4)_2\text{HPO}_4$, 1.0 mL/min).

We then performed a pilot study to estimate very basic characteristics of the pharmacokinetics of the new radiotracer via dynamic small-animal PET imaging with [^{18}F]9 in female CD-1 mice. The time–activity curves (TACs) obtained in different tissues under both baseline (administration of vehicle, $n = 2$) and blocking (administration of compound 2, $n = 2$) conditions are presented in Figure 3; the whole-body maximum intensity projections are shown in Figure S3 in the Supplementary Material. The overall biodistribution of [^{18}F]9 under baseline conditions corresponded to the known quite ubiquitous but physiologically not very dense expression of $\text{A}_{2\text{B}}$ receptors [25]. Although higher levels of the $\text{A}_{2\text{B}}$ receptor protein have been reported in the literature for certain cell types, such as alveolar epithelial cells and endothelial cells [3,25], the resemblance of the TACs in peripheral organs such as lungs under baseline and blocking conditions indicated no target-specific retention of [^{18}F]9 (TAC peak SUV_{lung}: 3.09 and 2.88 vs. 2.30 and 1.57, resp.; SUV_{60 min p.i., lung}: 0.44 and 0.25 vs. 0.32 and 0.20, resp.). This was slightly different to the results of Petroni et al. obtained for the carbon-11-labeled compound [^{11}C]4 in rats [13], because those authors described a significant decrease of uptake of [^{11}C]4 in the lung induced by the pretreatment of the $\text{A}_{2\text{B}}$ receptor agonist BAY60-6583. This discrepancy between our and Petroni’s results might indicate differences in the biological effects exerted by agonistic (BAY60-6583) or antagonistic (compound 2) $\text{A}_{2\text{B}}$ receptor ligands, as well as

model-related differences such as the expression of A_{2B} receptors. The latter option could also explain the about 10-fold lower uptake of [¹⁸F]9 in the brown adipose tissue (BAT) of female CD-1 mice in comparison to the uptake of [¹¹C]-4 in the BAT of male Wistar rats [13].

The time–activity distribution in the kidney, along with the concentration of activity determined in the urine during the metabolism study, indicated a renal excretion route of the radiotracer. In addition, the remarkably high and constantly increasing uptake determined in the gall bladder under blocking conditions indicated accumulation of [¹⁸F]9 in the bile, promoted by compound 2. A low tracer accumulation was detected in the brain, with an initial TAC peak SUV of 0.19 (0.20 and 0.17) and subsequent slow washout to an SUV of 0.11 (0.14 and 0.08) after 60 min p.i. Co-administration of compound 2 resulted in a slight reduction of the brain uptake, with a TAC peak SUV of 0.12 (0.11 and 0.13).

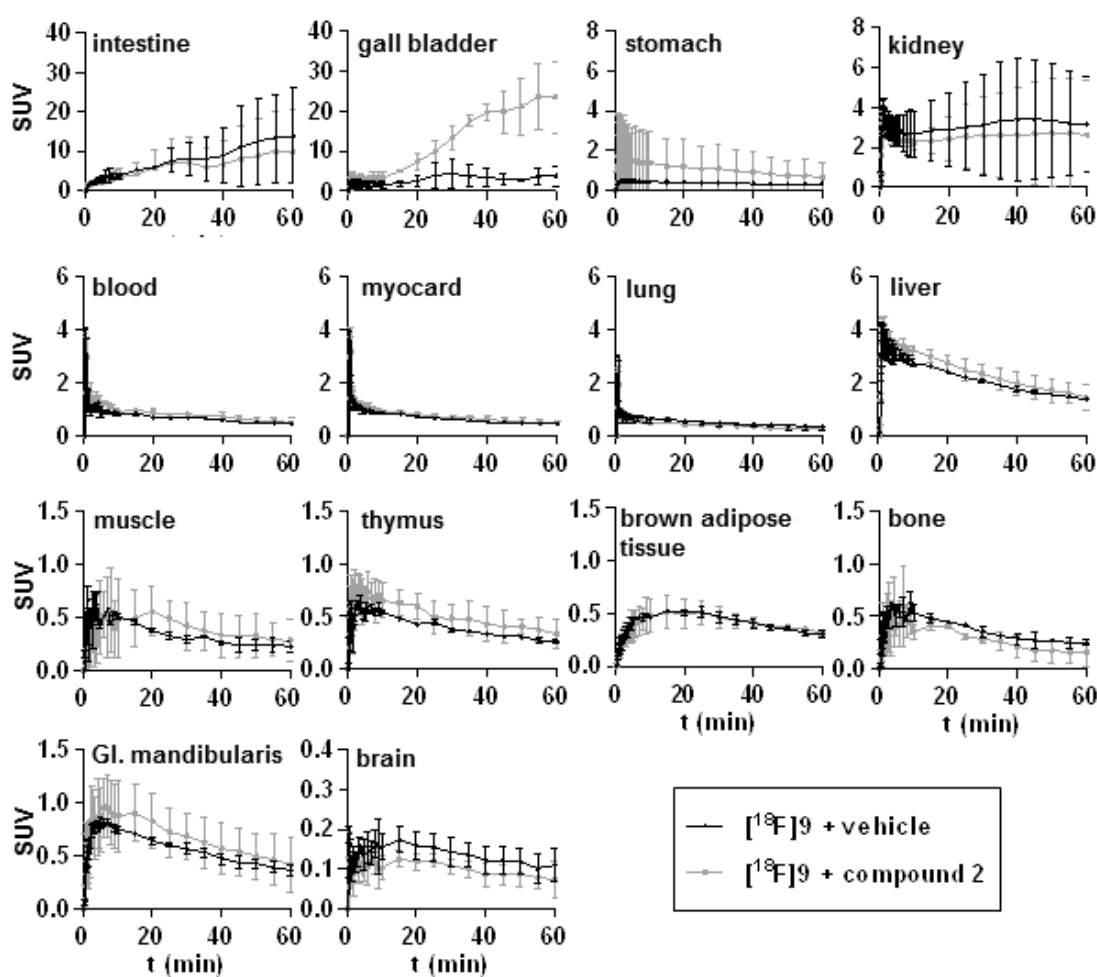


Figure 3. Biodistribution of [¹⁸F]9 in female CD-1 mice derived by small-animal PET over 60 min; time–activity curves (TACs) for tissue uptake are expressed as standard uptake values (SUVs), $n = 2$, mean \pm SD.

Although this study was performed in healthy animals, thus in an animal model not characterized by disease-related high expressions of A_{2B} receptors, these initial results are promising regarding a low non-specific binding of [¹⁸F]9 under physiological conditions. Accordingly, [¹⁸F]9 seems to be applicable for imaging of A_{2B} receptors in future studies in disease models, e.g., of inflammation or cancer. However, further studies are required in order to answer open questions such as the unexpected increase of activity in the gall bladder after pretreatment with antagonist 2.

3. Materials and Methods

3.1. Organic Chemistry

3.1.1. General

Analysis of all compounds was performed via mass spectroscopy (MS), thin-layer chromatography (TLC), and NMR spectroscopy. The final compounds **2**, **9**, and **10** were also subjected to HPLC analysis.

High-resolution mass spectra were recorded on an ESI-qTOF Impact II (Bruker Daltonik GmbH, Leipzig, Germany) and on an ESI-TOF micrOTOF (Bruker Daltonik GmbH, Leipzig, Germany) using ElectroSpray Ionization (ESI). NMR spectra (^1H , ^{13}C , ^{13}C -APT, ^{19}F , H,H-COSY, HSQC, HMBC) were recorded on spectrometers from Varian and Bruker. Splitting patterns are designated herein as follows: s: singlet, d: doublet, bs: broad singlet, dd: doublet of doublet.

Analytical TLC was performed on silica gel-coated plates (ALUGRAM SIL G/UV₂₅₄, Machery-Nagel, Düren, Germany). The spots were identified using a UV lamp or by spraying a solution of 0.1% ninhydrin in ethanol/water 1/10 or dipping into a KMnO_4 solution (3 g KMnO_4 , 20 g K_2CO_3 , 0.25 ml glacial acid, 300 ml water).

For purification of final products, flash-column chromatography was used with silica gel ZEOsorb 60/40-63 μm from Apollo Scientific Ltd., Cheshire, UK and silica gel 40-63 μm from VWR International GmbH, Darmstadt, Germany.

The chemical purity of the final compounds was $\geq 96\%$ and was controlled by HPLC using a $150 \times 3 \text{ mm}$ Reprisil-Pur Basic HD 3 μm column (Dr. Maisch HPLC GmbH, Ammerbuch-Entingen, Germany). These analytical chromatographic separations were performed on a Dionex Ultimate 3000 system, incorporating a LPG-3400SD pump, an autosampler WPS-3000 TSL, a column compartment TCC-3000SD, a diode array detector DAD3000 (monitoring from 254–720 nm), and a low-resolution mass spectrometer MSQ 3000 (Thermo Fisher Scientific, Darmstadt, Germany). A mixture of acetonitrile (ACN) and aqueous 20 mM NH_4OAc was used as eluent in a linear gradient system (0–2.5 min at 25% ACN, 2.5–11.0 min up to 95% ACN, 11.0–13.0 min at 95% ACN, 13.0–13.5 min up to 25% ACN, 13.5–15.0 min at 25%) with a flow of 0.6 mL/min.

Chemical names of compounds were generated using ChemDraw Professional 17.0 (PerkinElmer Informatics, Waltham, MA, USA).

3.1.2. 7-(Furan-2-yl)-6-(pyrimidin-4-yl)pyrido[2,3-*d*]pyrimidine-2,4-(1*H*,3*H*)-dione (**2**)

Compound **2** was synthesized according to the procedures reported by Eastwood et al. [16,17].

^1H NMR ($\text{DMSO-}d_6$, 300 MHz) δ : 6.60 (dd, $J = 3.5, 1.7 \text{ Hz}$, 1 H), 6.86 (dd, $J = 3.5, 0.8 \text{ Hz}$, 1 H), 7.48 (dd, $J = 5.2, 1.4 \text{ Hz}$, 1 H), 7.66 (dd, $J = 1.7, 0.8 \text{ Hz}$, 1 H), 8.28 (s, 1 H), 8.81 (d, $J = 5.2 \text{ Hz}$, 1H), 9.21 (d, $J = 1.3 \text{ Hz}$, 1 H), 11.52 (s, 1H), 11.89 (s, 1H) ppm. ^{13}C NMR ($\text{DMSO-}d_6$, 75 MHz) δ : 108.9, 112.9, 114.8, 121.9, 126.2, 139.5, 146.0, 150.1, 150.9, 151.6, 152.7, 157.6, 158.9, 162.1, 164.2 ppm. HRMS (ESI+) m/z calcd. for $\text{C}_{15}\text{H}_{10}\text{O}_3\text{N}_5^+$ $[\text{M}+\text{H}]^+$ 308.07782, found 308.07765.

3.1.3. Compounds **3–6**

These compounds were synthesized as described in the Supplementary Material.

3.1.4. 2-Amino-5-bromo-6-(furan-2-yl)nicotinamide (**7**)

A suspension of compound **6** (0.74 g, 2.8 mmol) in 22 mL ethanol, 15 mL water, 9.3 mL 6M aqueous NaOH and 0.8 mL H_2O_2 (50% in H_2O , 14.0 mmol) was stirred for 5 h at 50 °C. Afterwards, 200 mL water was added and the mixture was extracted with ethyl acetate ($4 \times 25 \text{ mL}$). The combined organic phases were dried over sodium sulfate, filtered, and the solvent was removed under reduced pressure. The obtained residue was purified by column chromatography (SiO_2 , ethyl acetate/*n*-hexane, 2/1, *v/v*) to obtain **7** with a yield of 45% (0.36 g, 1.26 mmol).

^1H NMR (DMSO- d_6 , 400 MHz) δ : 6.69 (dd, $J = 3.5, 1.8$ Hz, 1 H), 7.35 (dd, $J = 3.5, 0.8$ Hz, 1 H), 7.46 (bs, 3 H), 7.90 (d, $J = 0.9$ Hz, 1 H), 8.09 (bs, 1 H); 8.28 (s, 1H) ppm. ^{13}C NMR (DMSO- d_6 , 100 MHz) δ : 100.1, 109.5, 112.3, 114.6, 142.9, 145.0, 147.3, 151.0, 157.6, 168.6 ppm. HRMS (ESI+) m/z calcd. for $\text{C}_{10}\text{H}_9\text{O}_2\text{N}_3^{79}\text{Br}^+$ $[\text{M}+\text{H}]^+$ 281.98727, $\text{C}_{10}\text{H}_8\text{O}_2\text{N}_3^{79}\text{BrNa}^+$ $[\text{M}+\text{Na}]^+$ 303.96921, found 281.98678, 303.96892.

3.1.5. 6-Bromo-7-(furan-2-yl)pyrido[2,3-*d*]pyrimidine-2,4(1*H*,3*H*)-dione (8)

To a solution of **7** (100 mg, 0.35 mmol) in 2 mL dimethyl sulfoxide (DMSO), sodium hydride (35.4 mg, 0.88 mmol, 60% in oil) was added and the mixture was stirred for 30 min at room temperature. Afterwards, *N,N*-carbonyldiimidazole (CDI, 60 mg, 0.39 mmol) dissolved in 1 mL *N,N*-dimethylformamide (DMF) was added and the reaction mixture heated at 90 °C for two hours. After cooling to room temperature, the solution was treated with 100 mL aqueous 1M HCl and extracted with ethyl acetate (4 × 25 mL). The combined organic phases were dried over sodium sulfate, filtered, and the solvent was removed under reduced pressure. The obtained residue was purified by column chromatography (SiO_2 , $\text{CH}_2\text{Cl}_2/\text{CH}_3\text{OH}$, 39/1, *v/v*) to obtain **8** with a yield of 50% (55 mg, 0.18 mmol).

^1H NMR (DMSO- d_6 , 400 MHz) δ : 6.78 (dd, $J = 3.6, 1.8$ Hz, 1 H), 7.58 (d, $J = 3.6$ Hz, 1 H), 8.04 (d, $J = 1.4$ Hz, 1 H), 8.40 (s, 1 H), 11.55 (s, 1H), 11.87 (s, 1 H) ppm. ^{13}C NMR (DMSO- d_6 , 100 MHz) δ : 108.4, 110.2, 112.9, 117.0, 142.0, 146.5, 149.5, 149.7, 150.2, 151.2, 161.5 ppm. HRMS (ESI-) m/z calcd. for $\text{C}_{11}\text{H}_5\text{O}_3\text{N}_3^{79}\text{Br}^-$ $[\text{M}-\text{H}]^-$ 305.95198, found 305.95750.

3.1.6. 6-(2-Fluoropyridin-4-yl)-7-(furan-2-yl)pyrido[2,3-*d*]pyrimidine-2,4(1*H*,3*H*)-dione (9)

Compound **8** (50 mg, 0.16 mmol) was dissolved in 5 mL 1,4-dioxane together with 0.8 mL (1.60 mmol) of a 2 M Cs_2CO_3 solution and 2-(fluoropyridin-4-yl)boronic acid (34 mg, 0.24 mmol). The mixture was evacuated three times under reduced pressure and refilled with argon to remove air. Subsequently, $[\text{Pd}(\text{dppf})\text{Cl}_2]$ (12 mg, 0.016 mmol) was added under argon and the resulting suspension was stirred at 90 °C for two hours. After cooling to room temperature, the solution was treated with 100 mL aqueous 1 M HCl and extracted with ethyl acetate (4 × 25 mL). The combined organic phases were dried over sodium sulfate, filtered, and the solvent was removed under reduced pressure. The obtained residue was pre-purified by column chromatography (SiO_2 , $\text{CH}_2\text{Cl}_2/\text{CH}_3\text{OH}$ /ethyl acetate, 99/1/1, *v/v/v*) to obtain 31 mg (0.06 mmol, 59%) of crude **9**, which was then purified by semi-preparative HPLC (Reprosil-Pur Basic C18-HD, 250 × 20 mm, 35% ACN/aq. 20 mM NH_4OAc , flow 7.5 mL/min, $t_{\text{R}} \sim 17$ –19 min).

^1H NMR (DMSO- d_6 , 400 MHz) δ : 6.60 (d, $J = 3.6$ Hz, 1H), 6.75 (d, $J = 3.5$ Hz, 1H), 7.24 (s, 1H), 7.29 (d, $J = 5.1$ Hz, 1H), 7.74 (s, 1H), 8.13 (s, 1H), 8.27 (d, $J = 5.2$ Hz, 1H), 11.71 (bs, 2H) ppm. ^{13}C NMR (DMSO- d_6 , 100 MHz) δ : 108.6, 110.2 (d, $^2J_{\text{C,F}} = 38.5$ Hz), 112.9, 115.4, 123.0 (d, $^4J_{\text{C,F}} = 3.9$ Hz), 125.7 (d, $^4J_{\text{C,F}} = 3.5$ Hz), 139.3, 146.1, 147.8 (d, $^3J_{\text{C,F}} = 15.7$ Hz), 149.6, 150.9, 151.4, 152.4, 152.8 (d, $^3J_{\text{C,F}} = 8.4$ Hz), 162.1, 163.7 (d, $^1J_{\text{C,F}} = 235.3$ Hz) ppm. ^{19}F NMR (DMSO- d_6 , 376 MHz) δ : -68.6 ppm. HRMS (ESI-) m/z calcd. for $\text{C}_{16}\text{H}_8\text{O}_3\text{N}_4\text{F}^-$ $[\text{M}-\text{H}]^-$ 323.05859, found 323.05896.

3.1.7. 7-(Furan-2-yl)-6-(2-nitropyridin-4-yl)pyrido[2,3-*d*]pyrimidine-2,4(1*H*,3*H*)-dione (10)

4-Bromo-2-nitropyridine (200 mg, 1.0 mmol), 4,4,4',4',5,5,5',5'-octamethyl-2,2'-bis(1,3,2-dioxaborolane) (250 mg, 1.0 mmol), KOAc (560 mg, 5.0 mmol), and $[\text{Pd}(\text{dppf})\text{Cl}_2]$ (37 mg, 0.05 mmol) were suspended in 2 mL 1,4-dioxane under an inert atmosphere and the reaction mixture was heated to 90 °C. After an hour, the reaction mixture was cooled to room temperature and compound **8** (307 mg, 1.0 mmol), $[\text{Pd}(\text{dppf})\text{Cl}_2]$ (37 mg, 0.05 mmol), and Cs_2CO_3 (3.25 g, 10.0 mmol) were added under inert atmosphere and heated for an hour at 90 °C. After cooling to room temperature, the suspension was filtered over celite, the solvent was removed under reduced pressure, and the residue was purified by column chromatography (SiO_2 , $\text{CH}_2\text{Cl}_2/\text{CH}_3\text{OH}$, 99.5/0.5 to 98/2, *v/v*) to give **10** with a yield of 9% (31 mg, 0.088 mmol).

^1H NMR (DMSO- d_6 , 400 MHz) δ : 11.95 (s, 1H), 11.58 (s, 1H), 8.72 (d, $J = 4.9$ Hz, 1H), 8.31 (d, $J = 1.4$ Hz, 1H), 8.25 (s, 1H), 7.88 (dd, $J = 4.9, 1.5$ Hz, 1H), 7.71 (d, $J = 1.6$ Hz, 1H), 6.88 (d, $J = 3.5$ Hz, 1H), 6.62 (dd, $J = 3.5, 1.7$ Hz, 1H) ppm. ^{13}C NMR (DMSO- d_6 , 100 MHz) δ : 162.1, 157.2, 152.6, 151.4, 151.3, 150.9, 149.6, 149.2, 146.3, 139.9, 130.6, 124.9, 118.9, 115.6, 113.0, 108.7 ppm. HRMS (ESI+): m/z calcd. for $\text{C}_{16}\text{H}_9\text{N}_5\text{NaO}_5$ $[\text{M}+\text{Na}]^+$ 374.0496, found 374.0506.

3.2. In Vitro Radioligand Binding Experiments

Membrane preparations of recombinant CHO or HEK (human embryonic kidney) cells expressing the respective human adenosine receptor subtype were obtained according to Borrmann et al. [26] or purchased from Perkin Elmer, Germany. Radioligand binding assays using human A_1 , $\text{A}_{2\text{A}}$, $\text{A}_{2\text{B}}$ and A_3 receptors were performed according to Alnouri et al. [27].

The following radioligands were employed:

$[\text{^3H}]2\text{-Chloro-}N^6\text{cyclopentyladenosine}$ ($[\text{^3H}]CCPA$, molar activity: 58 Ci/mmol, 1 nM [28]) for the A_1 receptor,

$[\text{^3H}]3\text{-}(3\text{-hydroxypropyl})\text{-}7\text{-methyl-}8\text{-}(m\text{-methoxystyryl})\text{-}1\text{-propargylxanthine}$, ($[\text{^3H}]MSX\text{-}2$, molar activity: 84 Ci/mmol, 1 nM [29]) for the $\text{A}_{2\text{A}}$ receptor,

$[\text{^3H}]8\text{-}(4\text{-}[4\text{-}(4\text{-chlorophenyl})\text{piperazine-}1\text{-sulfonyl}]phenyl)\text{-}1\text{-propyl-}2,3,6,7\text{-tetrahydro-}1H\text{-purine-}2,6\text{-dione}$ ($[\text{^3H}]PSB\text{-}603$, molar activity: 73 Ci/mmol, 0.3 nM [26]) for the $\text{A}_{2\text{B}}$ receptor, and

$[\text{^3H}](R)\text{-}8\text{-ethyl-}4\text{-methyl-}2\text{-}(phenyl)1,4,7,8\text{-tetrahydro-}5H\text{-imidazo}[2,1\text{-}i]\text{purin-}5\text{-one}$ ($[\text{^3H}]PSB\text{-}11$, molar activity: 53 Ci/mmol, 1 nM [30]) for the A_3 receptor. Three separate experiments were performed to determine the K_i values. All data were analyzed with GraphPad Prism, Version 4.1 (GraphPad Inc., La Jolla, CA, USA).

3.3. Radiochemistry

3.3.1. General

No-carrier-added $[\text{^18F}]$ fluoride was produced via the $[\text{^18O}(p,n)\text{^18F}]$ nuclear reaction by irradiation of an $[\text{^18O}]\text{H}_2\text{O}$ target (Hyox 18 enriched water, Rotem Industries Ltd, Arava, Israel) on a Cyclone 18/9 (IBA RadioPharma Solutions, Lourain-La-Neuve, Belgium) with a fixed energy proton beam using a Nirta $[\text{^18F}]$ fluoride XL target.

Analytical chromatographic separations were performed on a JASCO LC-2000 system, incorporating a PU-2080Plus pump, AS-2055Plus auto injector (100 μL sample loop), and a UV-2070Plus detector (JASCO Deutschland GmbH, Pfungstadt, Germany) coupled with a gamma radioactivity HPLC detector (Gabi Star, raytest Isotopenmessgeräte GmbH, Straubenhardt, Germany). Data analysis was performed with Galaxie chromatography software (Agilent Technologies Deutschland GmbH, Waldbronn, Germany) using the chromatograms obtained at 254 nm. A Reprosil-Pur C18-AQ column (250 \times 4.6 mm; 5 μm ; Dr. Maisch HPLC GmbH; Ammerbuch-Entingen, Germany) with ACN/20 mM NH_4OAc aq. (pH 6.8) as eluent mixture and a flow of 1.0 mL/min was used (gradient: eluent A 10% ACN/20 mM aq. NH_4OAc ; eluent B 90% ACN/20 mM aq. NH_4OAc ; 0–5 min 100% A, 5–25 min up to 50% B, 25–26 min up to 100% B, 26–30 min 100% B, 30–31 min up to 100% A and 31–40 min 100% A).

The ammonium acetate and sodium dodecyl sulfate (SDS) concentrations stated as aq. 20 mM NH_4OAc and aq. 100 mM, respectively, correspond to the concentrations in the aqueous component of an eluent mixture.

3.3.2. Radiosynthesis

Remote-controlled radiosynthesis of $[\text{^18F}]\mathbf{9}$ was performed using a TRACERlab FX2 N synthesizer (GE Healthcare, Waukesha, WI, USA) equipped with a Laboport vacuum pump N810.3FT.18 (KNF Neuberger GmbH, Freiburg, Germany), a BlueShadow UV detector 10D (KNAUER GmbH, Berlin, Germany), and the TRACERlab FX Software (GE Healthcare, Waukesha, WI, USA).

[¹⁸F]Fluoride (2–7 GBq) was trapped on a Sep-Pak Accell Plus QMA Carbonate Plus light cartridge (Figure 4, entry 1, Waters GmbH, Eschborn, Germany) and eluted into the reactor with 400 µL of an aqueous solution of potassium carbonate (K₂CO₃, 1.8 mg, 13 µmol, entry 2). After addition of Kryptofix 2.2.2. in 1.5 mL ACN (11 mg, 29 µmol, entry 3), the mixture was azeotropically dried for approximately 10 min. Thereafter, 0.5–0.6 mg of the nitro precursor (**10**) dissolved in 800 µL DMSO (entry 4) was added, and the reaction mixture was stirred at 120 °C for 15 min. After cooling, the reaction mixture was diluted with 1.5 mL H₂O and 2.0 mL MeOH/H₂O 1/1 (*v/v*, entry 5) and transferred into the injection vial (entry 6). Semi-preparative HPLC was performed using a Reprosil-Pur 120 AQ column (250 × 20 mm; 10 µm; Dr. Maisch HPLC GmbH; Ammerbuch-Entingen, Germany) with a solvent composition of 60% MeOH/aq. 20 mM NH₄OAc at a flow rate of 8.0 mL/min (entry 7). [¹⁸F]**9** was collected in the dilution vessel (entry 8) previously loaded with 40 mL H₂O. Final purification was performed by passing the solution through a Sep-Pak[®] C18 light cartridge (entry 9), followed by washing with 2 mL water (entry 10) and elution of [¹⁸F]**9** with 1.3 mL EtOH (entry 11) into the product vial (entry 12). The ethanolic solution was transferred out of the hot cell and the solvent was reduced under a gentle argon stream at 70 °C to a final volume of 10–50 µL. Afterwards, the radiotracer was diluted in isotonic saline to obtain a final product containing 10% of EtOH (*v/v*).

The molar activity was determined on the basis of a calibration curve created under isocratic HPLC conditions (22% ACN/aq. 20 mM NH₄OAc; Reprosil-Pur 120 AQ 250 × 4.6 mm, flow 1.0 mL/min), using chromatograms obtained at 254 nm as an appropriate maximum of UV absorbance.

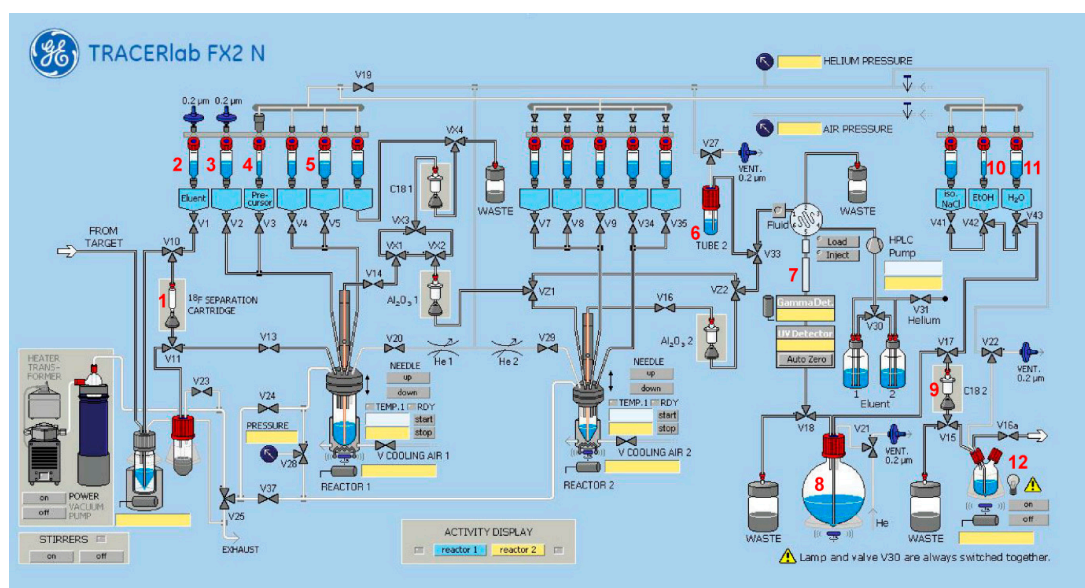


Figure 4. Scheme of the synthesis module TRACERlab FX2 N for the radiosynthesis of [¹⁸F]**9**. (1) Sep-Pak Accell Plus QMA Carbonate Plus light, (2) K₂CO₃ (1.8 mg in 400 µL water), (3) K₂2.2.2. (11 mg in 1.5 mL ACN), (4) precursor (0.5 mg of **10** in 800 µL DMSO), (5) 1.5 mL water and 2.0 mL MeOH/water, (6) injection vial, (7) Reprosil-Pur 120 AQ (60% MeOH/aq. 20 mM NH₄OAc, flow 8.0 mL/min), (8) 40 mL water, (9) Sep-Pak[®] C18 light, (10) 2 mL water, (11) 1.3 mL EtOH, (12) product vial.

The partition coefficient of [¹⁸F]**9** was experimentally determined for the *n*-octanol/PBS system by the shake-flask method as described previously [14].

3.4. In Vivo Studies in Mice

For metabolism studies (*n* = 2), [¹⁸F]**9** (30–40 MBq) was administered as a bolus in awake female CD-1 mice (10–12 weeks, 25–32 g) via the tail vein. At 30 min p.i., the animals were slightly anesthetized with isoflurane, and blood was sampled from retro-orbital plexus. Blood plasma was obtained as a supernatant after centrifugation of the whole blood samples (14,000 rpm, 1 min; Centrifuge 5418,

Eppendorf Vertrieb Deutschland GmbH, Wesseling-Berzdorf, Germany). After cervical luxation of the animals, urine samples were obtained. All samples were weighed and the respective activity measured in a dose calibrator (ISOMED 2010; MED Nuklear-Medizintechnik Dresden GmbH, Dresden, Germany).

MLC: For preparation of the MLC samples, mouse plasma (20–50 μ L) was dissolved in 200 μ L of 200 mM aq. sodium dodecyl sulfate (SDS) and injected into the MLC system. The MLC system was built up as described previously [14]. Separations were performed using a Reprosil-Pur C18-AQ column (250 \times 4.6 mm + 10 mm pre-column, particle size: 10 μ m) and an eluent mixture of EtOH/100 mM aq. SDS/25 mM (NH₄)₂HPO₄ in gradient mode (0–10 min at 100% 100 mM aq. SDS, 10–15 min up to 10% EtOH, 15–20 min at 10% EtOH, 20–21 min up to 100% 100 mM aq. SDS; 21–30 min at 100% 100 mM aq. SDS) at a flow rate of 1.0 mL/min. The same HPLC apparatus was used as described in the radiochemistry part in general.

RP-HPLC: Protein precipitation was performed by addition of an ice-cold mixture of ACN/water (9/1; *v/v*) in a ratio of 4:1 (*v/v*) of organic solvent to plasma. The sample workup was performed according to a procedure previously described in detail [14]. The urine samples were diluted with water and directly injected. To analyze the samples, the same HPLC apparatus and method was used as described in the radiochemistry section.

The biodistribution of the radiotracer was assessed in female CD-1 mice (30.6 \pm 0.4 g bodyweight) using a dedicated small-animal PET-MRI scanner (nanoScan, Mediso, Hungary) over 60 min followed by a subsequent T1-weighted MR. The anaesthetized (2% isoflurane, carrier gas mixture of 40% air and 60% O₂) female CD-1 mice were kept on a heated animal bed to maintain body temperature during imaging. Vehicle (10% DMSO in isotonic 0.9% NaCl solution) or compound **2** at 1 mg/kg bodyweight were co-injected with the tracer ([¹⁸F]**9**: injected dose of 6.9 \pm 0.1 MBq, equivalent to 10.4 \pm 0.9 fmol/g bodyweight) intravenously 20 seconds after starting the dynamic PET acquisition, performed in normal mode and with a coincidence mode 1–5. For subsequent dynamic reconstructions (Nucline v2.01, Mediso, Hungary) by Ordered Subset Expectation Maximization (OSEM3D) with an attenuation correction with four iterations, six subsets, and a voxel size of 0.4 mm³, list mode data were sorted into sinograms (12 \times 10 s, 6 \times 30 s, 5 \times 60 s, and 10 \times 300 s). PMOD software (v4.005, PMOD Technologies LLC, Zurich, Switzerland) was used for analysis of reconstructed studies and the results are expressed as standardized uptake value (SUV) given in mean \pm SD.

Animals for *in vivo* studies were obtained from the Medizinisch-Experimentelles Zentrum, Universität Leipzig. All procedures that included animals were approved by the respective State Animal Care and Use Committee and conducted in accordance with the German Law for the Protection of Animals (TVV 18/18 since 20 June 2018, DD24.1-5131/446/19, Landesdirektion Sachsen).

Supplementary Materials: Supplementary materials can be found at <http://www.mdpi.com/1422-0067/21/9/3197/s1>. Figure S1: Semi-preparative radio- and UV-HPLC chromatograms of [¹⁸F]**9**. Figure S2: Analytical radio- and UV-HPLC chromatograms of the final product of [¹⁸F]**9** spiked with the non-radioactive reference **9**. Figure S3. Maximum Intensity Projections (MIP) of mice treated with vehicle and compound **2** coinjected with [¹⁸F]**9**.

Author Contributions: C.E.M., B.W., M.L., W.D.-C., S.D.-S., C.J., J.S., P.B., conceived and designed the study; M.L. and R.-P.M. performed the organic syntheses; S.H. performed and analyzed the *in vitro* binding experiments; B.W. and R.T. performed the radiosyntheses and metabolite analysis; D.G. W.D.-C., S.D.-S., M.T. and P.B. performed and interpreted the *in vivo* studies; B.W., W.D.-C., M.L. and D.G. wrote the paper. All coauthors reviewed and revised the paper. All authors have read and agreed to the published version of the manuscript.

Funding: The authors would like to thank the BMBF (German Federal Ministry for Education and Research) for the financial support within the BioPharma initiative “Neuroallianz” (D11B project). Costs for publishing in open access are covered by the HZDR.

Acknowledgments: We are very thankful to K. Franke, A. Mansel and S. Fischer for providing [¹⁸F]fluoride. We are also thankful to L. Hennig, S. Billig, and R. Oehme from the University of Leipzig for measuring the NMR and high-resolution mass spectra. We thank A. Fischer and A. Püsche for performing radioligand binding assays.

Conflicts of Interest: The authors declare no conflict of interest. The founding sponsors had no role in the design of the study; in the collection, analyses, or interpretation of data; in the writing of the manuscript, and in the decision to publish the results.

References

1. Fredholm, B.B.; IJzerman, A.P.; Jacobson, K.A.; Linden, J.; Müller, C.E. International Union of Basic and Clinical Pharmacology. LXXXI. Nomenclature and Classification of Adenosine Receptors—An Update. *Pharmacol. Rev.* **2011**, *63*, 1–34. [[CrossRef](#)]
2. Fredholm, B.B.; IJzerman, A.P.; Jacobson, K.A.; Klotz, K.N.; Linden, J. International Union of Pharmacology. XXV. Nomenclature and classification of adenosine receptors. *Pharmacol. Rev.* **2001**, *53*, 527–552.
3. Feoktistov, I.; Biaggioni, I. Adenosine A_{2B} receptors. *Pharmacol. Rev.* **1997**, *49*, 381–402.
4. Fredholm, B.B.; Irenius, E.; Kull, B.; Schulte, G. Comparison of the potency of adenosine as an agonist at human adenosine receptors expressed in Chinese hamster ovary cells. *Biochem. Pharmacol.* **2001**, *61*, 443–448. [[CrossRef](#)]
5. Daly, J.W.; Butts-Lamb, P.; Padgett, W. Subclasses of adenosine receptors in the central nervous system: Interaction with caffeine and related methylxanthines. *Cell Mol. Neurobiol.* **1983**, *3*, 69–80. [[CrossRef](#)]
6. Müller, C.E.; Baqi, Y.; Hinz, S.; Namasivayam, V. Medicinal chemistry of A_{2B} adenosine receptors. In *The Adenosine Receptors*, Borea, P.A.; Varani, K., Gessi, S., Merighi, S., Vincenzi, F., Eds.; Humana Press: Totowa, NJ, USA, 2018; pp. 137–168.
7. Borea, P.A.; Gessi, S.; Merighi, S.; Vincenzi, F.; Varani, K. Pharmacology of Adenosine Receptors: The State of the Art. *Physiol. Rev.* **2018**, *98*, 1591–1625. [[CrossRef](#)] [[PubMed](#)]
8. Antonioli, L.; Blandizzi, C.; Pacher, P.; Hasko, G. Immunity, inflammation and cancer: A leading role for adenosine. *Nat. Rev. Cancer* **2013**, *13*, 842–857. [[CrossRef](#)] [[PubMed](#)]
9. Gao, Z.G.; Jacobson, K.A. A_{2B} Adenosine Receptor and Cancer. *Int. J. Mol. Sci.* **2019**, *18*, 5139. [[CrossRef](#)] [[PubMed](#)]
10. Sepulveda, C.; Palomo, I.; Fuentes, E. Role of adenosine A_{2B} receptor overexpression in tumor progression. *Life Sci.* **2016**, *166*, 92–99. [[CrossRef](#)]
11. Sorrentino, C.; Morello, S. Role of adenosine in tumor progression: Focus on A_{2B} receptor as potential therapeutic target. *J. Cancer Metastasis Treat.* **2017**, *3*, 127–138. [[CrossRef](#)]
12. Hinz, S.; Navarro, G.; Borroto-Escuela, D.; Seibt, B.F.; Ammon, Y.C.; de Filippo, E.; Danish, A.; Lacher, S.K.; Cervinkova, B.; Rafehi, M.; et al. Adenosine A_{2A} receptor ligand recognition and signaling is blocked by A_{2B} receptors. *Oncotarget* **2018**, *9*, 13593–13611. [[CrossRef](#)] [[PubMed](#)]
13. Petroni, D.; Giacomelli, C.; Taliani, S.; Barresi, E.; Robello, M.; Daniele, S.; Bartoli, A.; Burchielli, S.; Pardini, S.; Salvadori, P.A.; et al. Toward PET imaging of A_{2B} adenosine receptors: A carbon-11 labeled triazinobenzimidazole tracer: Synthesis and imaging of a new A_{2B} PET tracer. *Nucl. Med. Biol.* **2016**, *43*, 309–317. [[CrossRef](#)] [[PubMed](#)]
14. Lindemann, M.; Hinz, S.; Deuther-Conrad, W.; Namasivayam, V.; Dukic-Stefanovic, S.; Teodoro, R.; Toussaint, M.; Kranz, M.; Juhl, C.; Steinbach, J.; et al. Radiosynthesis and in vivo evaluation of a fluorine-18 labeled pyrazine based radioligand for PET imaging of the adenosine A_{2B} receptor. *Bioorg. Med. Chem.* **2018**, *26*, 4650–4663. [[CrossRef](#)] [[PubMed](#)]
15. Eastwood, P.; Esteve, C.; Gonzalez, J.; Fonquerna, S.; Aiguade, J.; Carranco, I.; Domenech, T.; Aparici, M.; Miralpeix, M.; Alberti, J.; et al. Discovery of LAS101057: A Potent, Selective, and Orally Efficacious A_{2B} Adenosine Receptor Antagonist. *ACS Med. Chem. Lett.* **2011**, *2*, 213–218. [[CrossRef](#)]
16. Eastwood, P.; Gonzalez, J.; Paredes, S.; Fonquerna, S.; Cardus, A.; Alonso, J.A.; Nueda, A.; Domenech, T.; Reinoso, R.F.; Vidal, B. Discovery of potent and selective bicyclic A_{2B} adenosine receptor antagonists via bioisosteric amide replacement. *Bioorg. Med. Chem. Lett.* **2010**, *20*, 1634–1637. [[CrossRef](#)]
17. Eastwood, P.; Gonzalez, J.; Paredes, S.; Nueda, A.; Domenech, T.; Alberti, J.; Vidal, B. Discovery of N-(5,6-diarylpyridin-2-yl)amide derivatives as potent and selective A_{2B} adenosine receptor antagonists. *Bioorg. Med. Chem. Lett.* **2010**, *20*, 1697–1700. [[CrossRef](#)]
18. Harada, H.; Asano, O.; Miyazawa, S.; Ueda, M.; Yasuda, M.; Yasuda, N. Aminopyridine Compounds and Use Thereof as Drugs. U.S. Patent 2004/006082, 1 August 2004.
19. Troschütz, R.; Dennstedt, T. Synthesis of Substituted 2-Aminonicotinonitriles. *Arch. Pharm.* **1994**, *327*, 33–40. [[CrossRef](#)]
20. Pham, S.M.; Chen, J.F.; Ansari, A.; Jadhavar, P.S.; Patil, V.S.; Khan, F.; Ramachandran, S.A.; Argaval, A.K.; Chakravarty, S. 1,8-Naphthyridinone Compounds and Uses Thereof. WO Patent 2019018583, 24 January 2019.

21. Miyaura, N.; Suzuki, A. Stereoselective Synthesis of Arylated (E)-Alkenes by the Reaction of Alk-1-Enylboranes with Aryl Halides in the Presence of Palladium Catalyst. *J. Chem. Soc. Chem. Comm.* **1979**, 866–867. [[CrossRef](#)]
22. Miyaura, N.; Yamada, K.; Suzuki, A. New Stereospecific Cross-Coupling by the Palladium-Catalyzed Reaction of 1-Alkenylboranes with 1-Alkenyl or 1-Alkynyl Halides. *Tetrahedron Lett.* **1979**, *20*, 3437–3440. [[CrossRef](#)]
23. Ishiyama, T.; Murata, M.; Miyaura, N. Palladium(O)-Catalyzed Cross-Coupling Reaction of Alkoxydiboron with Haloarenes—A Direct Procedure for Arylboronic Esters. *J. Org. Chem.* **1995**, *60*, 7508–7510. [[CrossRef](#)]
24. Khaledi, M.G. Micelles as separation media in high-performance liquid chromatography and high-performance capillary electrophoresis: Overview and perspective. *J. Chromatogr. A* **1997**, *780*, 3–40. [[CrossRef](#)]
25. Sun, Y.; Huang, P. Adenosine A_{2B} Receptor: From Cell Biology to Human Diseases. *Front. Chem.* **2016**, *4*, 37. [[CrossRef](#)] [[PubMed](#)]
26. Borrmann, T.; Hinz, S.; Bertarelli, D.C.; Li, W.; Florin, N.C.; Scheiff, A.B.; Müller, C.E. 1-Alkyl-8-(piperazine-1-sulfonyl)phenylxanthines: Development and characterization of adenosine A_{2B} receptor antagonists and a new radioligand with subnanomolar affinity and subtype specificity. *J. Med. Chem.* **2009**, *52*, 3994–4006. [[CrossRef](#)]
27. Alnouri, M.W.; Jepards, S.; Casari, A.; Schiedel, A.C.; Hinz, S.; Müller, C.E. Selectivity is species-dependent: Characterization of standard agonists and antagonists at human, rat, and mouse adenosine receptors. *Purinergic Signal.* **2015**, *11*, 389–407. [[CrossRef](#)]
28. Klotz, K.N.; Lohse, M.J.; Schwabe, U.; Cristalli, G.; Vittori, S.; Grifantini, M. 2-Chloro-N6-[³H]cyclopentyladenosine ([³H]CCPA)-a high affinity agonist radioligand for A₁ adenosine receptors. *Naunyn Schmiedebergs Arch. Pharmacol.* **1989**, *340*, 679–683. [[CrossRef](#)]
29. Müller, C.E.; Maurinsh, J.; Sauer, R. Binding of [³H]MSX-2 (3-(3-hydroxypropyl)-7-methyl-8-(m-methoxystyryl)-1-propargylxanthine) to rat striatal membranes-a new, selective antagonist radioligand for A_{2A} adenosine receptors. *Eur. J. Pharm. Sci.* **2000**, *10*, 259–265. [[CrossRef](#)]
30. Müller, C.E.; Diekmann, M.; Thorand, M.; Ozola, V. [³H]8-Ethyl-4-methyl-2-phenyl-(8R)-4,5,7,8-tetrahydro-1H-imidazo[2,1-i]-purin-5-one ([³H]PSB-11), a novel high-affinity antagonist radioligand for human A₃ adenosine receptors. *Bioorg. Med. Chem. Lett.* **2002**, *12*, 501–503. [[CrossRef](#)]



© 2020 by the authors. Licensee MDPI, Basel, Switzerland. This article is an open access article distributed under the terms and conditions of the Creative Commons Attribution (CC BY) license (<http://creativecommons.org/licenses/by/4.0/>).